Bearingless Torque Motor – Modeling and Control

Herbert Grabner*
Linz Center of Mechatronics
Shareholder of the ACCM GmbH
Linz, Austria

Siegfried Silber, Wolfgang Amrhein
Institute of Electrical Drives and Power Electronics
Johannes Kepler University Linz
Shareholder of the ACCM GmbH
Linz, Austria

Abstract

In recent years, demands for magnetically supported direct drives which operate contactless and feature a high torque capacity arise in industry. This paper presents an advantageous solution for a bearingless torque motor. The proposed configuration consists of a six phase winding configuration with concentrated coils in double star connection to keep power electronics efforts to a minimum. The six phase winding system generates simultaneously both, the actively controlled motor torque and the radial bearing forces for radial position control. The disk shaped hollow shaft rotor carries 26 permanent magnets. To reduce the systems costs, tilting deflection and the axial position of the rotor are stabilized passively by the magnetic reluctance forces. The mathematical model and an appropriate control for current and voltage drivers is introduced. Finally, the prototype motor is shown with special attention to the angle and rotor position sensor evaluation.

1 Introduction

The size of an electrical motor is largely determined by its torque rating. Hence, in many cases, the most compact and inexpensive solution is to combine a high speed machine with a gearbox. However, avoiding mechanical gears or other transmission elements has significant benefits: the system complexity and lubrication demand are reduced and additional losses and acoustic noise are eliminated. Today's industrial applications demand compact and efficient gearless motors (direct drives) to improve their reliability. This kind of electrical machine is referred to as torque motor characterized by small operating speed and high torque capacity per volume. In case of multi-pole PM torque motor systems, high efficiency, high dynamics and control precision with low maintenance costs can be realized [1, 2].

Furthermore, in chemical, biomedical or semiconductor industry, highly clean and tight environments are most important for certain processes. Thereby, many applications desire torque motor concepts, which operate contactless and are able to handle large mechanical stator-rotor-airgaps. Deploying magnetic bearing technology, these demanding requirements can be met and additionally lubrication is not needed anymore and there is no abrasive wear. However, magnetic bearings as well as bearingless (self-bearing) motor configurations are mainly designed for high speed applications [3, 4, 5, 6]. Therefore, they dispose of low pole numbers and reduced torque capacity. Recently, some magnetically levitated mutli-pole concepts with large rotor diameter have been introduced [7, 8], which fulfill the required demands.

This paper introduces a novel bearingless torque motor concept, shown in Fig. 1. The disk shaped hollow shaft rotor carries 26 permanent magnets. Due to the high PM flux density in the air gap, the axial position and tilting of the rotor are passively stabilized [9]. This guarantees a compact design with reduced complexity. The used concentrated stator winding configuration

*herbert.grabner@lcm.at, Linz Center of Mechatronics GmbH, Altenbergerstrasse 69, 4040 Linz, Austria, phone: +43 732 2468 6072, fax; +43 732 2468 6005

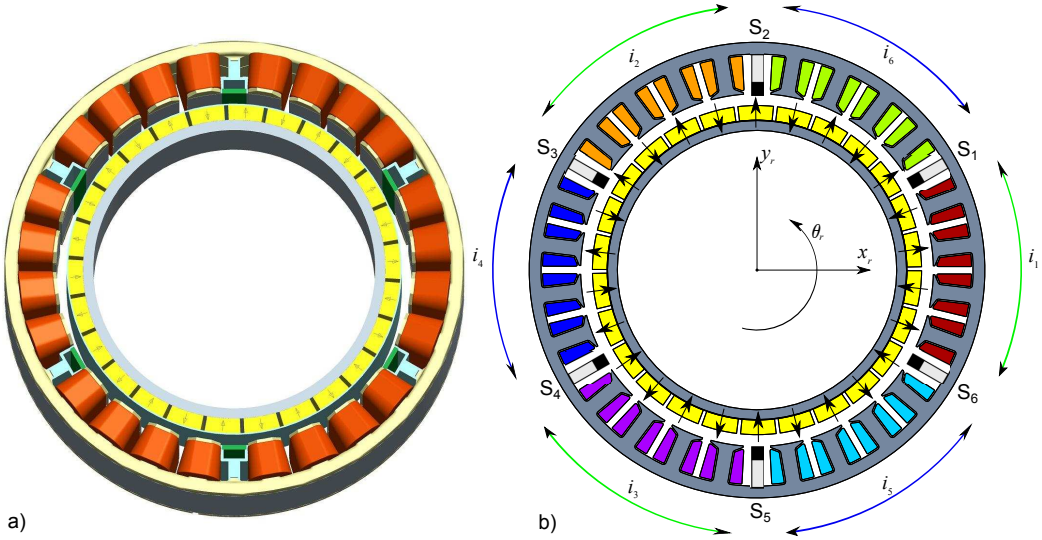

Figure 1: Bearingless torque motor. a) Arrangement. b) Cross section.

has a fundamental winding factor of almost one and small winding heads which implicates a high motor efficiency. Moreover, the six phase winding system generates simultaneously both, the actively controlled motor torque and the radial bearing forces in contrast to concepts with separated force and torque winding systems [10]. Generally, a five phase winding system would also be applicable [3], but has the disadvantage of an unused power half bridge when using two common three phase power modules. Furthermore, the six phase winding system provides the opportunity to use the space vector modulation technique with better DC link voltage utilization that decreases the necessary converter apparent power.

Due to simultaneous radial force and torque generation in all phase windings, the behavior of the bearingless torque motor is highly nonlinear. Thus, force and torque generation cannot be considered separately. In the following, modeling and control of a bearingless torque motor is presented.

2 Modeling

The basic configuration of the bearingless six-phase and 26 pole torque motor is illustrated in Fig. 1. Thereby, all four coils of one phase are serially connected and located in a stator division of 60°. The serial connection is strictly required since compensating currents due to unbalanced flux collection of the individual coils would circulate in a parallelly connected winding. Sensors for angular and radial position (S_1... S_6) are placed between the different phase sections. The rotor position with respect to the stator is referred to as x_r and y_r along with θ_r describing the rotor angle.

2.1 Force and Torque Model

The exact force and torque model of the bearingless torque motor is strongly nonlinear. Based on practical experience, some assumptions are applied in the following, where accuracy does

not suffer but mathematical handling will be improved.

If the rotor is not placed in the radial center, pull forces arise due to the destabilizing PM reluctance forces. As a result of the large air gap, small regarded eccentricity values and surface-mounted rotor magnets, they can be modeled as linear functions $F_{rx} = k_x x_r$, $F_{ry} = k_x y_r$ and the stiffness matrix is given by

$$\mathbf{K}_x = k_x \begin{bmatrix} 1 & 0 & 0 \\ 0 & 1 & 0 \\ 0 & 0 & 0 \end{bmatrix}, \tag{1}$$

where k_x is the stiffness constant. Generally, k_x depends on the electrical rotor angle θ_r, but due to the high number or rotor-poles k_x is angularly independent [11].

The electromagnetically generated force and torque values are quadratic functions of the phase currents. Using the mentioned assumptions leads to an almost linear dependency because the magnetic field from the winding system is small relative to the PM field. In addition, the influence of the stator slots, magnetic saturation as well as eddy current and hysteresis losses are not considered. The resulting relationships between current and force (F_{rx}, F_{ry}) as well as current and torque (T_r)

$$\begin{bmatrix} F_{rx} \\ F_{ry} \\ T_r \end{bmatrix} = \underbrace{\begin{bmatrix} T_{11}(\theta_r) & T_{12}(\theta_r) & T_{13}(\theta_r) & T_{11}(\theta_r) & T_{12}(\theta_r) & T_{13}(\theta_r) \\ T_{21}(\theta_r) & T_{22}(\theta_r) & T_{23}(\theta_r) & T_{21}(\theta_r) & T_{22}(\theta_r) & T_{23}(\theta_r) \\ T_{31}(\theta_r) & T_{32}(\theta) & T_{33}(\theta_r) & -T_{31}(\theta_r) & -T_{32}(\theta_r) & -T_{33}(\theta_r) \end{bmatrix}}_{\mathbf{T}_m(\theta_r)} \begin{bmatrix} i_1 \\ i_2 \\ i_3 \\ i_4 \\ i_5 \\ i_6 \end{bmatrix} \tag{2}$$

are nonlinear functions of θ_r, where F_{rx} and F_{ry} are the radial forces acting on the rotor and T_r specifies the motor torque. Furthermore, the vector of the phase currents can be written as

$$\mathbf{i} = \begin{bmatrix} i_1 & i_2 & i_3 & i_4 & i_5 & i_6 \end{bmatrix}^{\mathrm{T}} . \tag{3}$$

As shown in Fig. 1, the rotor magnets are radially magnetized ring segments that produce a rectangular field distribution. Due to the appropriate winding configuration, however, higher harmonics are canceled and an almost sinusoidal magnetomotive force (mmf) arises [12]. Thus, $\mathbf{T}_m(\theta_r)$ shows sinusoidal characteristic which decreases control efforts.

Setting up the equation of motion

$$\mathbf{M}\ddot{\mathbf{x}}_r = \mathbf{K}_x(\theta_r)\mathbf{x}_r + \mathbf{T}_m(\theta_r)\mathbf{i} , \tag{4}$$

where

$$\mathbf{x}_r = \begin{bmatrix} x_r & y_r & \gamma \end{bmatrix}^{\mathrm{T}} \tag{5}$$

defines the radial coordinates x_r, y_r and the mechanical rotor angle $\gamma = \frac{1}{p} \cdot \theta_r$, with p as the number of pole pairs. $\mathbf{M}$ is generally referred to as the mass matrix

$$\mathbf{M} = \begin{bmatrix} m_r & 0 & 0 \\ 0 & m_r & 0 \\ 0 & 0 & I_p \end{bmatrix} \tag{6}$$

with m_r being the mass of the hollow shaft rotor and I_p standing for the polar moment of inertia. Additional external damping is not considered, because it is application specific and has no influence on the proposed approach.

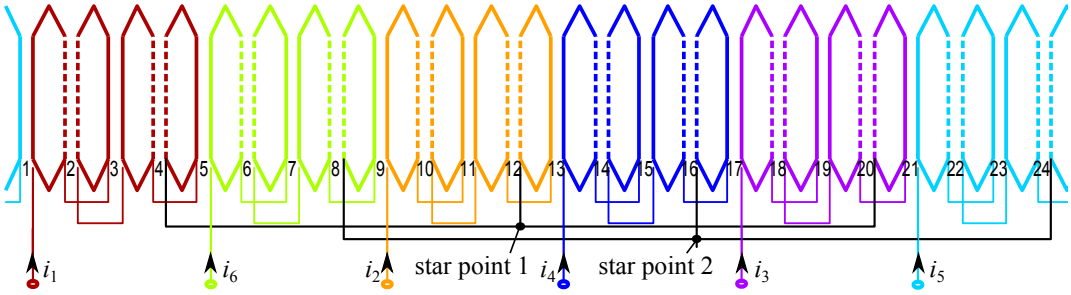

Figure 2: Winding configuration.

2.2 Electrical Model

Typically, bearingless torque motors are fed from a PWM voltage source inverter. Thus, terminal voltages instead of the phase currents form the control inputs

$$\mathbf{u} = \begin{bmatrix} u_1 & u_2 & u_3 & u_4 & u_5 & u_6 \end{bmatrix}^{\mathrm{T}} . \tag{7}$$

Then, current dynamics is determined by the stator voltage equation

$$\mathbf{u} = R\,\mathbf{i} + L\,\dot{\mathbf{i}} + \mathbf{T}_m^{\mathrm{T}}(\theta_r)\mathbf{v}_r . \tag{8}$$

Here, the velocities of the rotor in radial direction and the angular velocity are combined in

$$\mathbf{v}_r = \dot{\mathbf{x}}_r = \begin{bmatrix} v_x & v_y & \Omega_r \end{bmatrix}^{\mathrm{T}} . \tag{9}$$

In addition, a completely symmetrical motor design is assumed, which involves equal resistances R and equal self inductances $L_{xx} = L$. Furthermore, the coupling between the six phases can be neglected $L_{xy} = 0$.

2.3 Winding Configuration

The bearingless torque motor is composed of a six-phase winding system, where (2) shows how each phase current affects force and torque generation. However, an independent phase current control requires unconnected winding terminals, an independent current measurement and complex current or voltage drives per phase. Despite high costs, an independent phase control can be of increased significance in case of fault-tolerant bearingless motors [13].

Similar to conventional electrical machines, star connection can be applied reducing manufacturing and electronics complexity. Further simplification can be achieved by using two star points as illustrated in Fig. 2. This is possible because the mmf is sinusoidal and generating force and torque requires only certain field harmonics, where a double star connection is no constraint. Here, it is important to connect the phases in an appropriate way as given in Fig. 2 in order not to lose efficiency. For more details regarding the force and torque model please refer to [12].

3 Control with Current Driver

For the operation of the bearingless torque motor it is necessary to supply the six phases with such currents

$$\mathbf{i} = \mathbf{K}_m\left(\theta_r\right) \begin{bmatrix} F_{rx} \\ F_{ry} \\ T_r \end{bmatrix} \tag{10}$$

that the desired radial forces and torque are generated. The relation between the phase currents and the radial forces and torque is described in (2). The best set of phase currents in the sense of highest efficiency can be found by minimizing the resistive power losses which leads to

$$\mathbf{K}_m\left(\theta_r\right) = \mathbf{T}_m^{\mathrm{T}}\left(\mathbf{T}_m\mathbf{T}_m^{\mathrm{T}}\right)^{-1} \tag{11}$$

and further

$$\mathbf{K}_m\left(\theta_r\right) = \left(\mathbf{I} - \frac{1}{6}\mathbf{1}\mathbf{1}^{\mathrm{T}}\right)\mathbf{T}_m^{\mathrm{T}}\left(\mathbf{T}_m\left(\mathbf{I} - \frac{1}{6}\mathbf{1}\mathbf{1}^{\mathrm{T}}\right)\mathbf{T}_m^{\mathrm{T}}\right)^{-1} \tag{12}$$

for single star connection with $\mathbf{1} = \begin{bmatrix} 1 & 1 & \cdots & 1 \end{bmatrix}^{\mathrm{T}}$ and $\mathbf{I}$ as the identity matrix [14]. This optimization result can also be extended to the given bearingless torque motor with double star connection addressing the constraint

$$\sum_{k=1..3} i_k = \sum_{k=4..6} i_k = 0 \ , \tag{13}$$

which yields

$$\mathbf{K}_m\left(\theta_r\right) = \left(\mathbf{I} - \frac{1}{3}\begin{bmatrix} \mathbf{1}\mathbf{1}^{\mathrm{T}} & \mathbf{0} \\ \mathbf{0} & \mathbf{1}\mathbf{1}^{\mathrm{T}} \end{bmatrix}\right)\mathbf{T}_m^{\mathrm{T}}\left(\mathbf{T}_m\left(\mathbf{I} - \frac{1}{3}\begin{bmatrix} \mathbf{1}\mathbf{1}^{\mathrm{T}} & \mathbf{0} \\ \mathbf{0} & \mathbf{1}\mathbf{1}^{\mathrm{T}} \end{bmatrix}\right)\mathbf{T}_m^{\mathrm{T}}\right)^{-1} . \tag{14}$$

Equations (11), (12) and (14) show how different constraints concerning the winding schema can be fulfilled. However, if you bear in mind that efficiency is independent of the connection with zero, one or two star points then (11), (12) and (14) must show the same result for the given motor. This can easily be explained because the constraint introduced by (12) only locks the ability to generate a DC stator field, which will generally not be used for AC machines. Moreover, (2) shows symmetry, therefore (12) and (14) are equivalent. On these grounds, the double star connection can be applied without hesitation in order to decrease the necessary manufacturing and electronics effort. It is also the best choice when seen from the control side, because errors in current control are restricted to a minimum.

4 Control with Voltage Driver

To achieve the highest possible efficiency, bearingless motors are normally supplied with voltage source converters. However, the current control scheme (14) requires a current source instead of a voltage source. A feasible way of overcoming this problem is to use a nested current control loop for each motor phase. This control structure is usually called cascade control. The current control loop may either be implemented as an analog control system or a digital control system on a micro-controller or a DSP. In case of high electrical angular speeds $\omega_r = p \cdot \Omega_r$, which arise at the bearingless torque motor even at low mechanical speeds Ω_r due to a high pole number, a simple nested current control loop is not sufficient for high dynamic control. Thus, also the electrical model (8) will be taken into consideration.

4.1 Phase Transformation

First, the symmetry of (2) will be used to virtually split the windings into an independent bearing (force) and motor (torque) winding system. Using the transformation matrix in the form of

$$\mathbf{V}_E = \frac{1}{\sqrt{2}} \begin{bmatrix} \mathbf{I} & \mathbf{I} \\ \mathbf{I} & -\mathbf{I} \end{bmatrix} \tag{15}$$

results in a decoupled current to force relationship

$$\begin{bmatrix} F_{rx} \\ F_{ry} \\ T_r \end{bmatrix} = \mathbf{T}_m(\theta_r)\mathbf{V}_E\mathbf{i}_E = \sqrt{2} \begin{bmatrix} T_{11}(\theta_r) & T_{12}(\theta_r) & T_{13}(\theta_r) & 0 & 0 & 0 \\ T_{21}(\theta_r) & T_{22}(\theta_r) & T_{23}(\theta_r) & 0 & 0) & 0 \\ 0 & 0 & 0 & T_{31}(\theta_r) & T_{32}(\theta_r) & T_{33}(\theta_r) \end{bmatrix} \mathbf{i}_E \tag{16}$$

where

$$\mathbf{i}_E = \begin{bmatrix} i_{f,1} & i_{f,2} & i_{f,3} & i_{t,1} & i_{t,2} & i_{t,3} \end{bmatrix}^{\mathrm{T}} \tag{17}$$

denotes a new set of phase currents. Now, the Clarke transformation

$$\mathbf{V}_c = \begin{bmatrix} \mathbf{V}_{c1} & \mathbf{0} \\ \mathbf{0} & \mathbf{V}_{c2} \end{bmatrix} \tag{18}$$

with

$$\mathbf{V}_{c1} = \sqrt{\frac{2}{3}} \begin{bmatrix} 1 & -0.5 & -0.5 \\ 0 & -\frac{\sqrt{3}}{2} & \frac{\sqrt{3}}{2} \end{bmatrix}^{\mathrm{T}}, \mathbf{V}_{c2} = \sqrt{\frac{2}{3}} \begin{bmatrix} 1 & -0.5 & -0.5 \\ 0 & \frac{\sqrt{3}}{2} & -\frac{\sqrt{3}}{2} \end{bmatrix}^{\mathrm{T}} \tag{19}$$

can further reduce the complexity and leads to

$$\begin{bmatrix} F_{rx} \\ F_{ry} \\ T_r \end{bmatrix} = \mathbf{T}_m(\theta_r)\mathbf{V}_E\mathbf{V}_c\mathbf{i}_{DQ} = \begin{bmatrix} cos(\theta_r) & sin(\theta_r) & 0 & 0 \\ -sin(\theta_r) & cos(\theta_r) & 0 & 0 \\ 0 & 0 & -sin(\theta_r) & cos(\theta_r) \end{bmatrix} \begin{bmatrix} c_f\mathbf{I} & \mathbf{0} \\ \mathbf{0} & c_t\mathbf{I} \end{bmatrix} \mathbf{i}_{DQ} \tag{20}$$

where

$$\mathbf{i}_{DQ} = \begin{bmatrix} i_{f,D} & i_{f,Q} & i_{t,D} & i_{t,Q} \end{bmatrix}^{\mathrm{T}} \tag{21}$$

describing the resulting current components. The force and torque constants are given by c_f and c_t, respectively. Therefore, a total phase current transformation

$$\mathbf{i} = \mathbf{V}\mathbf{i}_{DQ} \tag{22}$$

with

$$\mathbf{V} = \mathbf{V}_E\mathbf{V}_c = \frac{1}{\sqrt{3}} \begin{bmatrix} 1 & 0 & 1 & 0 \\ -\frac{1}{2} & \frac{\sqrt{3}}{2} & -\frac{1}{2} & \frac{\sqrt{3}}{2} \\ -\frac{1}{2} & -\frac{\sqrt{3}}{2} & -\frac{1}{2} & -\frac{\sqrt{3}}{2} \\ 1 & 0 & -1 & 0 \\ -\frac{1}{2} & \frac{\sqrt{3}}{2} & \frac{1}{2} & -\frac{\sqrt{3}}{2} \\ -\frac{1}{2} & -\frac{\sqrt{3}}{2} & \frac{1}{2} & \frac{\sqrt{3}}{2} \end{bmatrix} \tag{23}$$

is applied. In order to get a fully invertible transformation (20) will be expanded with a field weakening component T_d, which results in

$$\begin{bmatrix} F_{rx} \\ F_{ry} \\ T_d \\ T_r \end{bmatrix} = \underbrace{\begin{bmatrix} c_f\mathbf{P}(\theta_r) & \mathbf{0} \\ \mathbf{0} & c_t\mathbf{P}(\theta_r) \end{bmatrix}}_{\overline{\mathbf{T}}_m(\theta_r)} \mathbf{i}_{DQ} \tag{24}$$

with the Park transformation

$$\mathbf{P}(\theta_r) = \begin{bmatrix} cos(\theta_r) & sin(\theta_r) \\ -sin(\theta_r) & cos(\theta_r) \end{bmatrix}. \tag{25}$$

Using field weakening, an operation above nominal speed can be realized when accepting higher copper losses and therefore, a reduced efficiency. Now, introducing the current components

$$\begin{bmatrix} i_{f,d} \\ i_{f,q} \end{bmatrix} = \mathbf{P}(\varphi) \begin{bmatrix} i_{f,D} \\ i_{f,Q} \end{bmatrix} \text{ and } \begin{bmatrix} i_{t,d} \\ i_{t,q} \end{bmatrix} = \mathbf{P}(\varphi) \begin{bmatrix} i_{t,D} \\ i_{t,Q} \end{bmatrix} \tag{26}$$

makes it possible to emphasize the similarity to field oriented control (FOC) of PMSM [15, 16]. The subscripts D and Q in (21) and (26) are used for direct and quadrature axis of the stator and d and q for the rotor components, respectively. Applying (24) results in

$$F_{rx} = c_f i_{f,d},\ F_{ry} = c_f i_{f,q} \text{ and } T_r = c_t i_{t,q}, \tag{27}$$

where a decoupled current to force and torque relationship is established. The transformation of the phase currents

$$\mathbf{i} = \mathbf{V} \begin{bmatrix} \mathbf{P}^{\mathrm{T}}(\theta_r) & \mathbf{0} \\ \mathbf{0} & \mathbf{P}^{\mathrm{T}}(\theta_r) \end{bmatrix} \mathbf{i}_{dq}$$

is invariant with respect to the electrical power, leading to the phase voltage transformation

$$\mathbf{u}_{dq} = \begin{bmatrix} \mathbf{P}(\theta_r) & \mathbf{0} \\ \mathbf{0} & \mathbf{P}(\theta_r) \end{bmatrix} \mathbf{V}^{\mathrm{T}}\mathbf{u}\ . \tag{28}$$

Applying (22) and (28) the stator voltage equation (8) can be rewritten in the form

$$\mathbf{u}_{dq} = R + L\dot{\mathbf{i}}_{dq} + \underbrace{\omega_r L \begin{bmatrix} 0 & -1 & 0 & 0 \\ 1 & 0 & 0 & 0 \\ 0 & 0 & 0 & -1 \\ 0 & 0 & 1 & 0 \end{bmatrix} \mathbf{i}_{dq} + \begin{bmatrix} c_f & 0 & 0 \\ 0 & c_f & 0 \\ 0 & 0 & 0 \\ 0 & 0 & c_u \end{bmatrix} \begin{bmatrix} \dot{x_r} \\ \dot{y_r} \\ \omega_r \end{bmatrix}}_{\mathbf{u}_{ind}}, \tag{29}$$

with the voltage constant $c_u = \frac{1}{p}c_t$. All nonlinear components arise from induced voltages and are summarized in $\mathbf{u}_{ind}$. With increasing rotor speed also the induced voltages increase and disturb the current control system, which is manly implemented with linear PI or PID (proportional-integral-derivative) controllers. Thus, $\mathbf{u}_{ind}$ should be added (feedforward) to the output of the current controllers in order to eliminate nonlinearity of the system.

4.2 Voltage Modulation

For the operation of the bearingless torque motor, variable voltage waveforms need to be created, and this is normally achieved by using a DC to AC converter. Arbitrary electric potentials at the inverter's terminals can be obtained by using pulse-width-modulation (PWM) techniques.

Generally, for three-phase star- or delta-connected motors space vector modulation (SVM) is quite common, which treats the three-phase inverter as a single unit [17]. SVM has the advantage of lower harmonics and a higher modulation index. Thus, DC bus voltage can be better utilized, which decreases the phase current demand of the power electronics. Due to the dual star connection, SVM can also be applied for the bearingless torque motor.

The reference voltage $\mathbf{u}_{dq,ref}$ must finally be transformed back according to

$$\mathbf{u} = \mathbf{V} \begin{bmatrix} \mathbf{P}^{\mathrm{T}}(\theta_r) & \mathbf{0} \\ \mathbf{0} & \mathbf{P}^{\mathrm{T}}(\theta_r) \end{bmatrix} \mathbf{u}_{dq,ref} = \mathbf{V}\mathbf{u}_{DQ,ref}. \tag{30}$$

Clearly, (30) can be directly used, but then SVM algorithms cannot be applied. It is more efficient to define

$$\mathbf{u} = \begin{bmatrix} \mathbf{V}_{c1} & \mathbf{0} \\ \mathbf{0} & \mathbf{V}_{c1} \end{bmatrix} \mathbf{u}^*_{DQ,ref} = \mathbf{V}^*_c \mathbf{u}^*_{DQ,ref} \tag{31}$$

with

$$\mathbf{u}^*_{DQ,ref} = \mathbf{V}^*_E \mathbf{u}_{DQ,ref}. \tag{32}$$

Concerning the implementation in software, $\mathbf{V}_{c1}$will be replaced with the SVM algorithm. The missing matrix $\mathbf{V}^*_{\mathbf{E}}$ is deduced from

$$\mathbf{V} = \mathbf{V}_E \mathbf{V}_c = \mathbf{V}^*_E \mathbf{V}^*_c \text{ and } \mathbf{V}^{\mathrm{T}}\mathbf{V} = \mathbf{I} \tag{33}$$

as

$$\mathbf{V}^*_E = \mathbf{V}^{*\mathrm{T}}_c \mathbf{V}_E \mathbf{V}_c = \frac{1}{\sqrt{2}} \begin{bmatrix} 1 & 0 & 1 & 0 \\ 0 & -1 & 0 & 1 \\ 1 & 0 & -1 & 0 \\ 0 & -1 & 0 & -1 \end{bmatrix}. \tag{34}$$

For the realization in hardware two standard three phase power modules can be applied. Due to (13) it is sufficient to measure two phase currents per subsystem in hardware, the remaining phase current can then be easily calculated. Moreover, current reconstruction techniques in the PWM inverters which require only one current sensor in the DC circuit (e.g. low side shunt) for each three phase system can be implemented, as illustrated in Fig. 3. The DC-link current depends on the states of the inverter switches. In each PWM period, there are two time slots, when one certain phase current can be determined out of the DC-link current measurement. If the current measurement is synchronized with the PWM pulses, two of the tree phase currents can be measured and the third one can be reconstructed out of the measured results. However, an effective and accurate measurement can only be achieved by sophisticated PWM patterns or additional mathematical observer methods [18, 19, 20].

4.3 Controller Implementation

The used control scheme is outlined in Fig. 4. The proposed control shows a high similarity to conventional FOC [15, 16]. Thus, it is also possible to use existing motor control software libraries with small extensions. In Fig. 4, reference values of force and torque are required which are typically provided by superimposed position and speed control. Thanks to the proposed feedback control, the system shows linearity and the main current controllers as well as controllers for position and speed can be defined separately by means of standard design methods. However, due to the given decoupled configuration, usually proportional-integral-derivative (PID) controllers are implemented because they have been successfully applied to many industrial applications. Moreover, the use of T_d allows flux weakening for an operation above nominal speed when accepting higher copper losses, and therefore, a lower efficiency [15, 16].

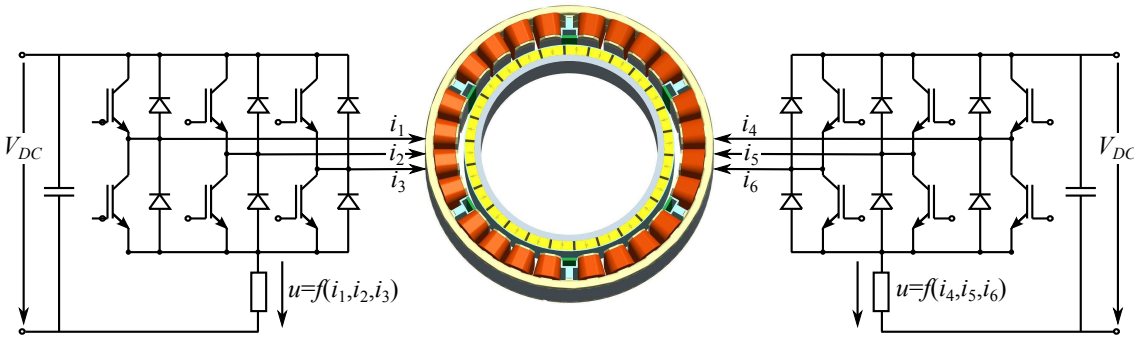

Figure 3: Current reconstruction technique in the PWM inverter.

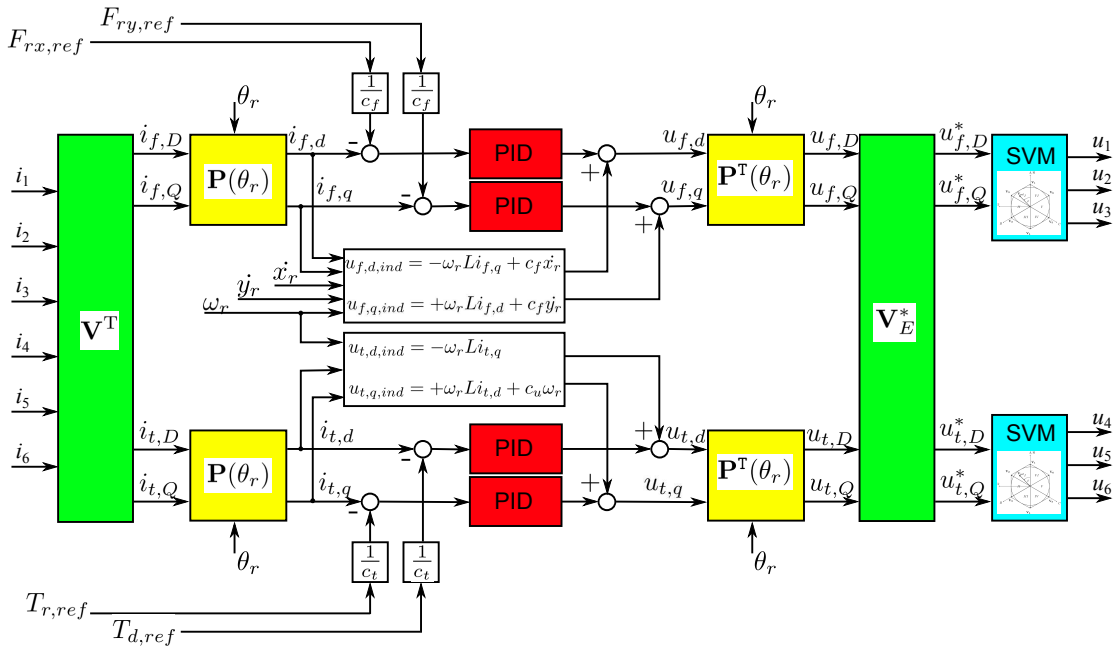

Figure 4: Block diagram of the proposed feedback control.

5 Experimental Setup

The setup of the bearingless torque motor is shown in Fig. 5. With an outer rotor diameter of 113 mm, a rotor height of 25 mm and a stator outer diameter of 155 mm this motor has a torque capacity of 5 Nm and a radial force capacity of 81 N at rated current. The air gap has a length of 4 mm. Concerning the rotor rare earth PM of grade 42M with 1.28 T remanence flux density are used. The rated speed of the motor is 1000 rpm leading to an output power of 523 W. The estimated efficiency based on finite element simulations is 87%.

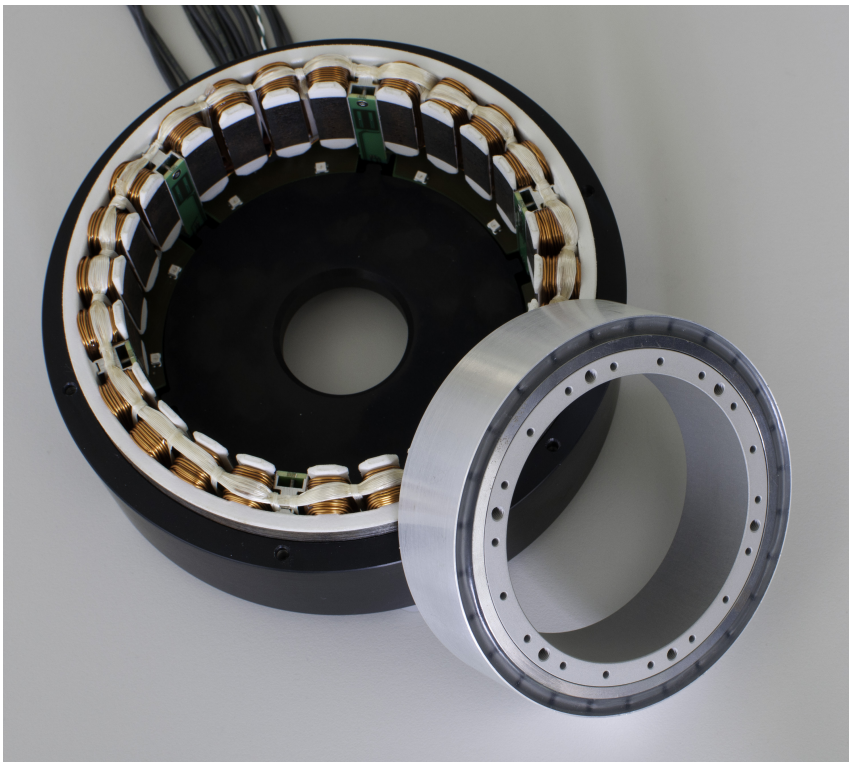

Figure 5: Prototyp of the bearingless torque motor.

5.1 Position and Angle Sensor Evaluation

Concerning the feedback control, the information of the radial position x_r, y_r and the angle θ_r of the rotor have to be provided. Thus, sensors have to be integrated into the motor. Typically, these sensors cannot be directly placed in the radial air gap due to the pole shoes which are commonly used to improve motor behavior. Thus, the construction becomes more complex and requires more space.

The proposed bearingless torque motor separates the phase windings in adjacent sectors without overlapping as shown in Fig. 1. Thereby, the sector margins can be enlarged and optimized to place sensors between two sectors [12]. Generally, the information of two sensors would be sufficient but the signals of six sensors can be transformed into two orthogonal components.

Eddy current sensors are used for contactless radial position detection. The position sensors are symmetrically placed around the circumference of the air gap in steps of 60° and the corresponding signals are summarized in

$$\mathbf{x}_s = \begin{bmatrix} x_{s1} & x_{s2} & x_{s3} & x_{s4} & x_{s5} & x_{s6} \end{bmatrix}^{\mathrm{T}}. \tag{35}$$

Using the transformation matrix

$$\mathbf{V}_{sens} = \frac{1}{3} \begin{bmatrix} \cos\left(\frac{\pi}{6}\right) & \cos\left(\frac{3\pi}{6}\right) & \cos\left(\frac{5\pi}{6}\right) & \cdots & \cos\left(\frac{11\pi}{6}\right) \\ \sin\left(\frac{\pi}{6}\right) & \sin\left(\frac{3\pi}{6}\right) & \sin\left(\frac{5\pi}{6}\right) & \cdots & \sin\left(\frac{11\pi}{6}\right) \end{bmatrix}, \tag{36}$$

the signal components of (35) are projected into orthogonal axes

$$\begin{bmatrix} x_r \\ y_r \end{bmatrix} = \mathbf{V}_{sens}\mathbf{x}_s. \tag{37}$$

For the rotor angle detection, hall sensors determine the PM magnetic field in the air gap. For sensor evaluation it is convenient to transform the signals to sine and cosine, respectively, in order to simplify the calculation of the angle by the arc tangent function. Again, the signals of the hall sensors are summarized in

$$\mathbf{h}_s = \begin{bmatrix} h_{s1} & h_{s2} & h_{s3} & h_{s4} & h_{s5} & h_{s6} \end{bmatrix}^{\mathrm{T}}. \tag{38}$$

The pitch between two hall sensors is $\gamma_h = 60^\circ$ mechanical angle or $\theta_h = p \cdot 60^\circ \hat{=} 60^\circ$ electrical angel, respectively. Thus, (36) can also be used to project (38) into orthogonal axes

$$\begin{bmatrix} h_x \\ h_y \end{bmatrix} = \mathbf{V}_{sens}\mathbf{h}_s \tag{39}$$

and the rotor angle results in

$$\theta_r = \arctan\left(\frac{h_y}{h_x}\right). \tag{40}$$

When applying (40), higher harmonics as well as a DC offset of h_x and h_y usually result in measurement errors. Due to the radially magnetized ring segments, the hall sensors detect rather a rectangular field and thus, the signal contains a lot of higher order harmonics. Using six sensor signals, these effects can strongly be limited. The transformation (36) suppresses a DC offset as well as the 2^{nd}, 3^{rd}, 4^{th},6^{th},8^{th},9^{th},10^{th},... harmonics, whereas the 1^{st}, 5^{th}, 7^{th}, 11^{th}, 13^{th}, ... harmonics are not affected by the chosen transformation. For further information concerning the theoretical background please refer to [21]. Moreover, the numerical evaluation of (36) yields

$$\mathbf{V}_{sens} = \frac{1}{6}\begin{bmatrix} \sqrt{3} & 0 & -\sqrt{3} & -\sqrt{3} & 0 & \sqrt{3} \\ 1 & 2 & 1 & -1 & -2 & -1 \end{bmatrix}, \tag{41}$$

where it can be seen that vis a vis placed sensor are evaluated differentially, which increases the linearity of the angle and position measurement.

6 Conclusion

This paper introduces a novel bearingless torque motor and deals with modeling and control. First, the mathematical model is derived which contains the force and torque as well as the electrical model. Then it is shown how to modulate the phase currents when using current drivers for different winding configurations. For best dynamics and highest total efficiency also the control with voltage drivers is proposed. Thereby, it turned out that with the help of phase current transformation, the control approach shows a high similarity to the FOC of a PMSM. Due to double star connection, two independent three phase power modules can be applied, using SVM for best utilization of DC bus voltage. Finally, a prototype motor is shown. Thanks to the phase windings being located in separated sectors, sensors can be effectively integrated. Based on redundant sensor placement, higher harmonics can be suppressed which leads to higher accuracy.

7 Acknowledgment

This work was mainly conducted within the research project “Nachhaltig ressourcenschonende elektrische Antriebe durch höchste Energie- und Material-Effizienz” (sustainable and resource-saving electrical drives through high energy and material efficiency) and is sponsered within the program of the European Union “Regionale Wettbewerbsfähigkeit OÖ 2007-2013 (Regio 13)” by the European Regional Development Fund (ERDF) and the Province of Upper Austria. Parts of the work have been carried out within the Austrian Center of Competence in Mechatronics (ACCM), which is part of the COMET K2 program of the Austrian Government.

References

[1] Y. Kano and N. Matsui. A design approach for direct-drive permanent-magnet motors. *Industry Applications, IEEE Transactions on*, 44(2):543 –554, march-april 2008.

[2] R. Wrobel and P.H. Mellor. Design considerations of a direct drive brushless machine with concentrated windings. *Energy Conversion, IEEE Transactions on*, 23(1):1 –8, march 2008.

[3] H. Grabner, W. Amrhein, S. Silber, and W. Gruber. Nonlinear feedback control of a bearingless brushless dc motor. *Mechatronics, IEEE/ASME Transactions on*, 15(1):40 –47, feb. 2010.

[4] H. Mitterhofer and W. Amrhein. Design aspects and test results of a high speed bearingless drive. In *Power Electronics and Drive Systems (PEDS), 2011 IEEE Ninth International Conference on*, pages 705 –710, dec. 2011.

[5] Y. Okada, N. Yamashiro, K. Ohmori, T. Masuzawa, T. Yamane, Y. Konishi, and S. Ueno. Mixed flow artificial heart pump with axial self-bearing motor. *Mechatronics, IEEE/ASME Transactions on*, 10(6):658 – 665, dec. 2005.

[6] S.-M. Yang and C.-W.. Chou. Experimental verification of radial force control for a pmsm self-bearing motor drive. In *IECON 2011 - 37th Annual Conference on IEEE Industrial Electronics Society*, pages 1854 –1859, nov. 2011.

[7] W. Gruber, T. Nussbaumer, H. Grabner, and W. Amrhein. Wide air gap and large-scale bearingless segment motor with six stator elements. *Magnetics, IEEE Transactions on*, 46(6):2438 –2441, june 2010.

[8] P. Karutz, T. Nussbaumer, W. Gruber, and J.W. Kolar. Novel magnetically levitated two-level motor. *Mechatronics, IEEE/ASME Transactions on*, 13(6):658 –668, dec. 2008.

[9] R. Schöb and N. Barletta. Principle and application of a bearingless slice motor. *JSMB (The Japan Society of Mechanical Engineers) International Journal*, 40(4):593–598, 1997.

[10] F. Zürcher, T. Nussbaumer, and J. W. Kolar. Motor torque and magnetic levitation force generation in bearingless brushless multipole motors. *Mechatronics, IEEE/ASME Transactions on*, PP(99):1 –10, 2011.

[11] C. Hüttner. Nonlinear state control of a left ventricular assist device. In *Proc. 8th International Symposium on Magnetic Bearings*, 2002.

[12] S. Silber, H. Grabner, W. Amrhein, and R. Lohninger. Design aspects of bearingless torque motors. In *Proc. 13th International Symposium on Magnetic Bearings*, 2012.

[13] W. Xiaolin, S. Wang, D. Zhiquan, and Y. Shengzou. Analysis of fault-tolerance control strategy of the single winding bearingless pm slice motor. In *Proc. 12th International Symposium on Magnetic Bearings*, 2010.

[14] S. Silber and W. Amrhein. Power optimal current control scheme for bearingless pm motors. In *Proc. 7th International Symposium on Magnetic Bearings*, 2000.

[15] P. Vas. *Sensorless Vector and Direct Torque Control*. Oxford Univ. Press, Oxford, U.K., 1998.

[16] R. Krishnan. *Electric Motor Drives*. Prentice Hall, New Jersey, 2001.

[17] H. M. Rashid. *Power Electronics*. Pearson Prentice Hall, Upper Saddle River, NJ, 2004.

[18] Jung-Ik Ha. Voltage injection method for three-phase current reconstruction in pwm inverters using a single sensor. *Power Electronics, IEEE Transactions on*, 24(3):767 –775, march 2009.

[19] Y. Cho, T. LaBella, and J.-S. Lai. A three-phase current reconstruction strategy with online current offset compensation using a single current sensor. *Industrial Electronics, IEEE Transactions on*, 59(7):2924 –2933, july 2012.

[20] D. P. Marcetic and E. M. Adzic. Improved three-phase current reconstruction for induction motor drives with dc-link shunt. *Industrial Electronics, IEEE Transactions on*, 57(7):2454 –2462, july 2010.

[21] W. Gruber, W. Amrhein, T. Stallinger, and H. Grabner. Bearingless segment motor with buried magnets. *Journal of System, Design and Dynamics*, 3(5):704–716, 2009.